Jurnal Riset Kimia

ISSN (print) : 1978-628X
ISSN (online) : 2476-8960

Synthesis of Copper Oxide from HKUST-1 and Its Applications for Removal of Congo Red

Izzah Maulidah[1] and Aep Patah[1*]

[1]Division of Inorganic and Physical Chemistry, Faculty of Mathematics and Natural Sciences, Institut Teknologi Bandung, Bandung, Indonesia

Corresponding Author:
Aep Patah
aep@itb.ac.id

Received: February 2025
Accepted: March 2026
Published: March 2026

©Aep Patah et al. This is an open-access article distributed under the terms of the Creative Commons Attribution License, which permits unrestricted use, distribution, and reproduction in any medium, provided the original author and source are credited.

Abstract

This study presents research findings on the synthesis and characterization of HKUST-1 and derived-copper oxide materials, with significant practical implications. The HKUST-1 was synthesized using the solvothermal method at 100 °C for 10 hours using copper nitrate trihydrate ($Cu(NO_3)_2{\cdot}3H_2O$) as the metal ion and trimesic acid as the ligand. The various copper oxides, CuO (air), $Cu/Cu_2O/C$ (Ar), and CuO (Ar/O_2) were produced through pyrolysis from HKUST-1 at 600 °C for 8 hours. X-ray Diffraction (XRD) analysis confirmed the characteristic peaks of HKUST-1 and the other copper oxides. Pyrolysis under argon yielded a $Cu/Cu_2O/C$ (Ar) mixture instead of CuO. Fourier Transform Infrared (FTIR) spectroscopy showed consistent absorption bands while Scanning Electron Microscopy (SEM) revealed that HKUST-1 and derived HKUST-1 copper oxides had an octahedral crystal morphology. UV-DRS analysis demonstrated that CuO derived HKUST-1 exhibited smaller band gap as compared to the pure CuO sample. Adsorption tests with a 50 ppm Congo Red (CR) solution showed that all materials reached optimal adsorption at 60 minutes, with $Cu/Cu_2O/C$ (Ar) achieving the highest capacity of 95,52 mg/g. In photocatalysis tests, CuO (Ar/O_2) removed 53% of contaminants, outperforming commercial CuO at 29%. The $Cu/Cu_2O/C$ (Ar) composite demonstrated the highest removal rate at 99%, indicating its potential for practical applications.

Keywords: *Adsorption; Congo red; copper oxide; Cu-MOF; HKUST-1.*

Introduction

The rational design of functional inorganic materials with controlled morphology and composition at the micro and nanoscale has attracted considerable interest, driving the development of innovative synthetic approaches. Metal oxides are one of the inorganic materials that have garnered significant attention in various applications, such as gas sensors, electronic devices, and photocatalysis[1]. Photocatalysis is a promising approach for environmental remediation, particularly for the degradation of pollutants in aquatic systems. Under light irradiation, the photocatalyst generates electron-hole pairs that produce reactive oxygen species (ROS), such as •OH and $\bullet O_2^-$, which efficiently oxidize organic pollutants into less harmful products[2]. Compared to conventional methods such as adsorption[3] and coagulation[4], photocatalysis offers superior efficiency through direct oxidative degradation rather than phase transfer.

Congo red is an anionic azo dye extensively discharged from domestic and industrial activities. Its persistence and accumulation in aquatic environments pose significant ecological and toxicological risks due to its complex aromatic structure and high chemical stability[5]. Photocatalytic degradation is an effective

DOI: https://doi.org/10.25077/jrk.v17i1.822

process where light generates reactive species that break the azo (-N=N-) bonds and aromatic structures of Congo red molecules[6]. Several metal oxide-based photocatalysts have been developed and widely investigated for their application in the photocatalytic degradation of Congo red, such as zinc oxide (ZnO)[7], titanium dioxide[8], manganese oxide (MnO_2)[9], and copper oxide (CuO)[10]. Among these materials, CuO has attracted considerable attention owing to its facile synthesis, low toxicity, and natural abundance. Morphological control of photocatalysts has emerged as a key strategy to enhance their performance, as structural features strongly influence light absorption, charge separation, and surface reaction kinetics. Lim et al. demonstrated that tuning the NaOH concentration during synthesis enables precise control over the morphology of ZnO as a precursor for Ag/ZnO, yielding five distinct structural forms. Among these, the spherical flower-like ZnO exhibited the highest photocatalytic activity, highlighting the strong correlation between morphology and catalytic performance[11]. Similarly, Jalali et al. reported that the photocatalytic properties of ZnO/CuO composites can be effectively modulated through pH-controlled synthesis. Increasing the pH not only promoted the formation of CuO nanoflower structures but also significantly reduced the band gap energy, resulting in enhanced photocatalytic activity compared to pristine CuO[12]. Therefore, the ability to control the shape and/or composition of CuO during the synthesis process is crucial to ensure its optimal performance.

Metal-organic frameworks (MOFs) are novel porous materials composed of hybrid organic and inorganic compounds, formed by metal ion clusters with various organic linkers. MOFs have proven to be ideal templates or precursors for creating porous transition metal oxide materials through solid-state heating processes under controlled conditions. This is due to the orderly arrangement of metal and organic elements in MOF structures, which feature distinct pores[13],[14]. The conversion of MOFs into metal oxides through thermal processes in the solid state (such as calcination and pyrolysis) is a technique where the metal components in MOFs serve as an intrinsic source for producing metal oxides that retain similar shapes and structural features to the parent MOFs. This method offers a simple and well-controlled pathway to fabricate metal oxides with novel and unique compositional and structural features[15],[16]. For instance, Sáenz et al. reported the successful synthesis of ZnO nanoparticles derived from Zeolitic Imidazolate Frameworks (ZIF-8) via direct calcination, demonstrating that the intrinsic dodecahedral morphology of ZIF-8 was preserved even after calcination at 1000 °C, resulting in enhanced adsorption performance[17]. Furthermore, the synthesis of MOF-derived metal oxides can be effectively controlled by tuning the heating rate and calcination atmosphere. Li et al. demonstrated that varying the heating rate of HKUST-1 (Hong Kong University of Science and Technolog) led to the formation of mixed-valence CuO/Cu_2O, while preserving the octahedral morphology of the parent framework, which was strongly correlated with enhanced photocatalytic denitrification activity[18]. Henri et al. investigated the synthesis of ZnO under various calcination atmospheres (N_2,O_2, and air), which led to significant differences in morphology and crystallinity. Notably, the sample calcined in air demonstrated the highest photocatalytic performance in the degradation of Rhodamine B[19]. In their study, Xiaodong Zhang and co-workers prepared Mn_2O_3 catalysts from Mn-MOFs under different pyrolysis atmospheres and demonstrated that sequential pretreatment in Ar and subsequently in O_2 maximized the Mn^{3+} content and surface-adsorbed oxygen, thereby enhancing catalytic activity relative to catalysts exposed to a single atmosphere[20].

Therefore, the development of low-cost oxide materials, particularly CuO, via a MOF-derived pyrolysis strategy remains an important challenge. In this study, CuO was synthesized from HKUST-1 under different atmospheric conditions (air, Ar, and Ar/O_2) to systematically elucidate the influence of the calcination atmosphere on morphology, crystallinity, and catalytic performance. The resulting materials were evaluated for their adsorption capacity and

photocatalytic efficiency toward the removal of Congo Red (CR), providing insights into the structure–activity relationship of MOF-derived CuO.

Experimental

Materials

The materials used in this study include 1,3,5-benzenetricarboxylic acid (H_3BTC, Sigma-Aldrich), copper(II) nitrate trihydrate ($Cu(NO_3)_2{\cdot}3H_2O$), ethanol (C_2H_5OH, Merck, 99,9%), N,N-dimethylformamide (DMF, Merck, 99,5%), demineralized water (Amidis), argon gas (Ar), a mixture of argon and oxygen gas (Ar/O_2), commercial copper(II) oxide (CuO), and Congo Red ($C_{32}H_{22}N_6Na_2O_6S_2$, Merck, 99,8%).

Instruments

For the characterization process, the following instruments were used: X-Ray Diffraction (XRD, Philips, PW1701), Fourier Transform Infrared (FTIR) spectroscopy, Scanning Electron Microscopy (SEM, JSM, 6510 LV), Energy Dispersive X-Ray Spectroscopy (EDX), and UV-Vis spectrophotometer.

Methods

Synthesis of HKUST-1

HKUST-1 was synthesized by the solvothermal method with several modifications based on a previously reported procedure[21]. The synthesis was carried out by dissolving 1.02 gram of $Cu(NO_3)_2{\cdot}3H_2O$ in 7.5 mL of demineralized water. Subsequently, 0.50 gram of H_3BTC was dissolved in an ethanol:DMF mixture at a 1:1 (v/v) ratio, using 7.5 mL of the mixture in a separate container. The mixture was then heated in an oven for a solvothermal process at 100 °C for 10 hours. Afterward, the mixed solution was cooled to room temperature and left undisturbed for 48 hours. The resulting precipitate was washed by soaking in 15 mL of DMF for 24 hours. The precipitate was then decanted and soaked in 15 mL of methanol in an oil bath at a temperature of 50–55 °C for 3 days. The final precipitate was dried in an oven at 80°C for 4 hours.

Synthesis of Copper Oxide

HKUST-1 needs to be converted into copper oxide through the pyrolysis process. A total of 0.50 gram of HKUST-1 was placed in a calcine boat and inserted into a tubular furnace. The calcination process was carried out at 600 °C for 8 hours[22]. The variations in the atmosphere, including air, Ar, and Ar/O_2. The variation was introduced during the calcination process by flowing different gases over the sample.

Adsorption Test

A contact time variation test was conducted to determine the optimum adsorption time. The test was performed on all synthesized materials. A total of 10 mg of the synthesized material was placed in a beaker, followed by the addition of 20 mL of CR solution with an initial concentration of 50 mg/L. The contact time variation test was carried out in the dark with constant stirring at 300 rpm. The contact time variations used in this study were 10, 20, 30, 40, 50, 60, and 70 minutes. The solution was then centrifuged at 1500 rpm for 20 minutes. The resulting filtrate was analyzed using a UV-Vis spectrophotometer at a maximum wavelength of 498 nm.

Photocatalysis Test

The photocatalysis for CR removal under visible light irradiation began by weighing 0.01 gram of material, followed by adding 20 mL of CR solution into a beaker. The photocatalytic test was then conducted in a photocatalytic reactor under visible light with constant stirring at 300 rpm. The time variations used in this study were 20, 40, 60, 80, and 100 minutes. After the photocatalytic process, the solution was centrifuged at 1500 rpm for 20 minutes. The resulting filtrate from the photocatalytic process was analyzed using a UV-Vis spectrophotometer at a maximum wavelength of 498 nm.

Results and Discussion

The diffractograms of HKUST-1 and copper oxide were identified based on the XRD results, as shown in Fig. 1.

DOI: https://doi.org/10.25077/jrk.v17i1.822

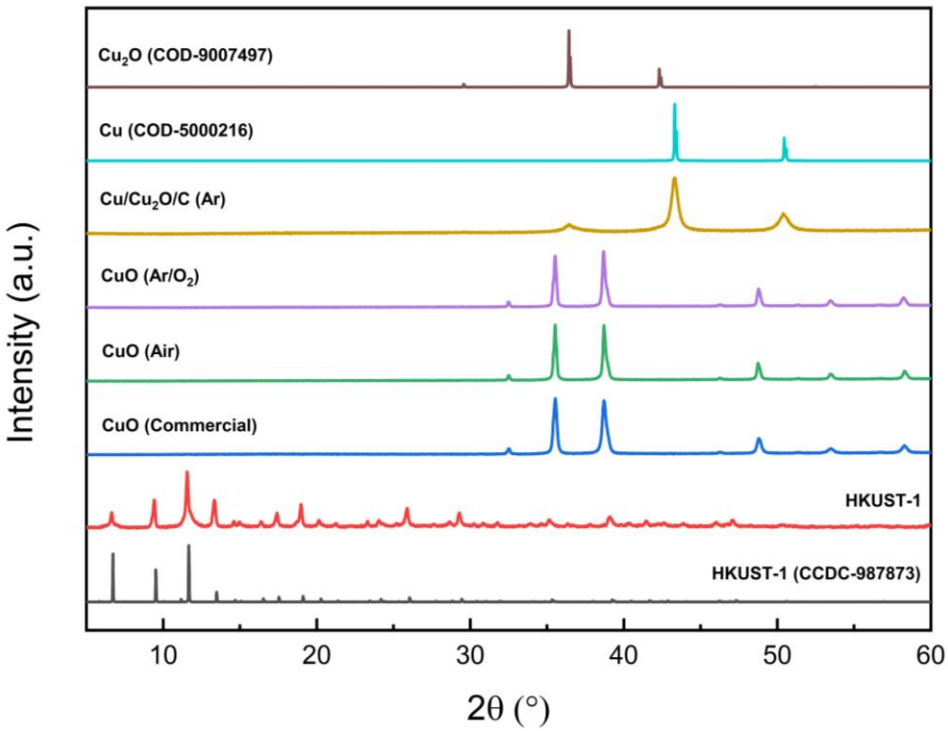

Figure 1. XRD patterns of the synthesized materials.

The synthesized HKUST-1 exhibited characteristic diffraction peaks at 6.66°, 9.51°, 11.61°, and 13.32°[21]. In the diffractograms of commercial CuO, CuO (air), and CuO (Ar/O_2), the characteristic peaks of HKUST-1 were no longer observed. Instead, new diffraction peaks appeared at 35.53° and 38.73°, corresponding to the characteristic planes of CuO[10]. These results confirm that CuO was successfully synthesized from HKUST-1 via the calcination process.

However, HKUST-1 calcined under an argon atmosphere did not exhibit the characteristic peaks of CuO. Instead, diffraction peaks appeared at 43.29° and 50.36°, corresponding to metallic Cu (COD-5000216). This result indicates that Cu^{2+} in the Cu-MOF was successfully reduced to zero-valent Cu during the high-temperature calcination process, with carbon acting as the reducing agent. A diffraction peak at 36.40° was also observed, which corresponds to Cu_2O (COD 9007497). This may be attributed to incomplete reduction by carbon. The Cu/Cu_2O/C (Ar) diffraction peak at 36.34° was not clearly distinguishable, likely due to the relatively low content of Cu_2O in the Cu/Cu_2O/C (Ar) composite[23]. Under an inert argon atmosphere, the direct formation of CuO is unlikely because of the insufficient oxygen availability required to oxidize Cu to CuO. Instead, carbon monoxide (CO) and hydrocarbon species (C–H) generated from the decomposition of the organic ligands act as reducing agents, converting Cu^{2+} to Cu_2O and subsequently to metallic Cu. Consequently, a Cu/Cu_2O/C (Ar) composite is formed[24].

The FTIR spectrum of HKUST-1 (Fig. 2) exhibits characteristic absorption bands consistent with previous reports[21]. A broad band at 3425.44 cm^{-1} is attributed to O–H stretching vibrations, originating from adsorbed water molecules or residual hydroxyl groups associated with the H_3BTC ligand. The band at 1622.77 cm^{-1} corresponds to the aromatic C=C stretching vibration of the benzene ring. Furthermore, the bands at 1444.02 and 1368.21 cm^{-1} are assigned to the asymmetric and symmetric stretching vibrations of the carboxylate (COO^-) groups, confirming the coordination of the BTC ligand within the framework. The absorption bands observed at 721.84 and 487.31 cm^{-1} are attributed to Cu–O vibrations, indicating the formation of metal–oxygen bonds in the structure. For

commercial CuO, CuO (air), Cu/Cu_2O/C (Ar), and CuO (Ar/O_2), the spectra display absorption bands at similar wavenumbers, corresponding to O–H, C–O, and Cu–O vibrations[25].

The surface morphology of HKUST-1 (Fig. 3) exhibits a well-defined octahedral structure with large crystal size and sharp edges, consistent with previous reports [21]. Commercial CuO displays a predominantly spherical morphology with an irregular surface texture. In contrast, CuO (air) and CuO (Ar/O_2) largely retain the octahedral morphology of HKUST-1, although noticeable agglomeration is observed and the structural preservation is not uniform across all particles. This phenomenon is attributed to the uncontrolled heating rate during the pyrolysis process. A rapid temperature increase accelerates the decomposition of organic components in the precursor, resulting in significant volume contraction while partially preserving the initial framework morphology, which ultimately promotes particle agglomeration[18]. Notably, the Cu/Cu_2O/C (Ar) sample clearly maintains a distinct octahedral morphology similar to that of HKUST-1, although several crack defects are visible on the particle surface.

EDX analysis was performed to determine the elemental composition of the synthesized materials, and the results are summarized in Table 1. The as-synthesized HKUST-1 consists primarily of Cu, C, and O elements, where Cu originates from the $Cu(NO_3)_2 \cdot 3H_2O$ precursor, while C and O are derived from the H_3BTC ligand. After pyrolysis, all samples still contain Cu, C, and O elements, although their relative percentages vary significantly. The CuO (air), Cu/Cu_2O/C (Ar), and CuO (Ar/O_2) samples exhibit an increased Cu content accompanied by a substantial decrease in C and O percentages. This change is attributed to the thermal decomposition of the organic ligand during pyrolysis, where carbon- and hydrogen-containing species are released as volatile products such as CO_2, CO, and H_2O vapor.

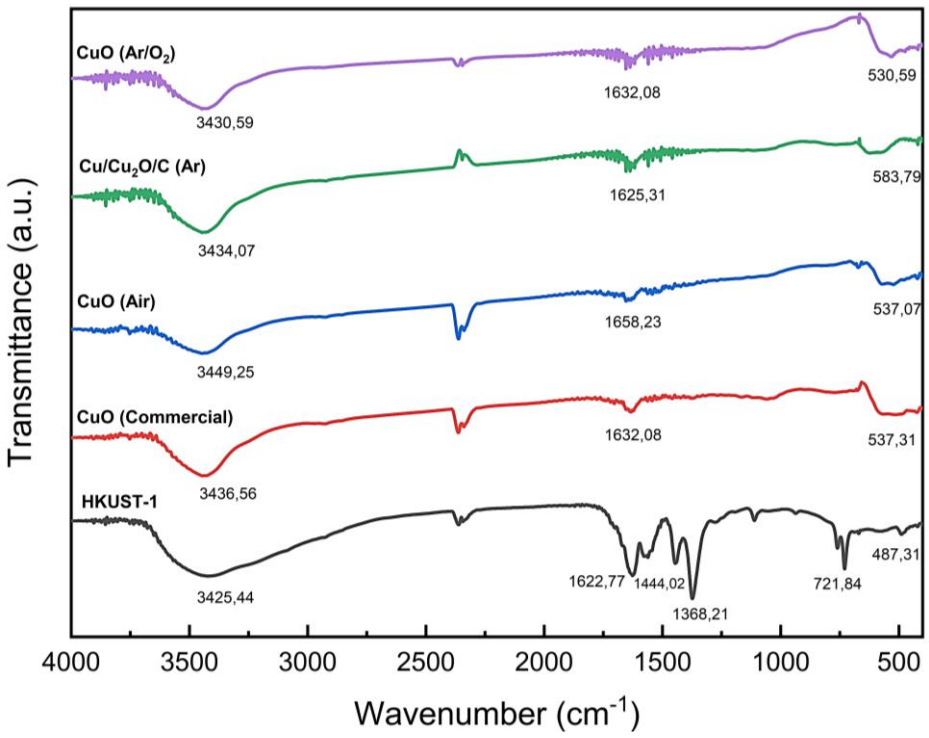

Figure 2. FTIR spectra of the synthesized materials

DOI: https://doi.org/10.25077/jrk.v17i1.822

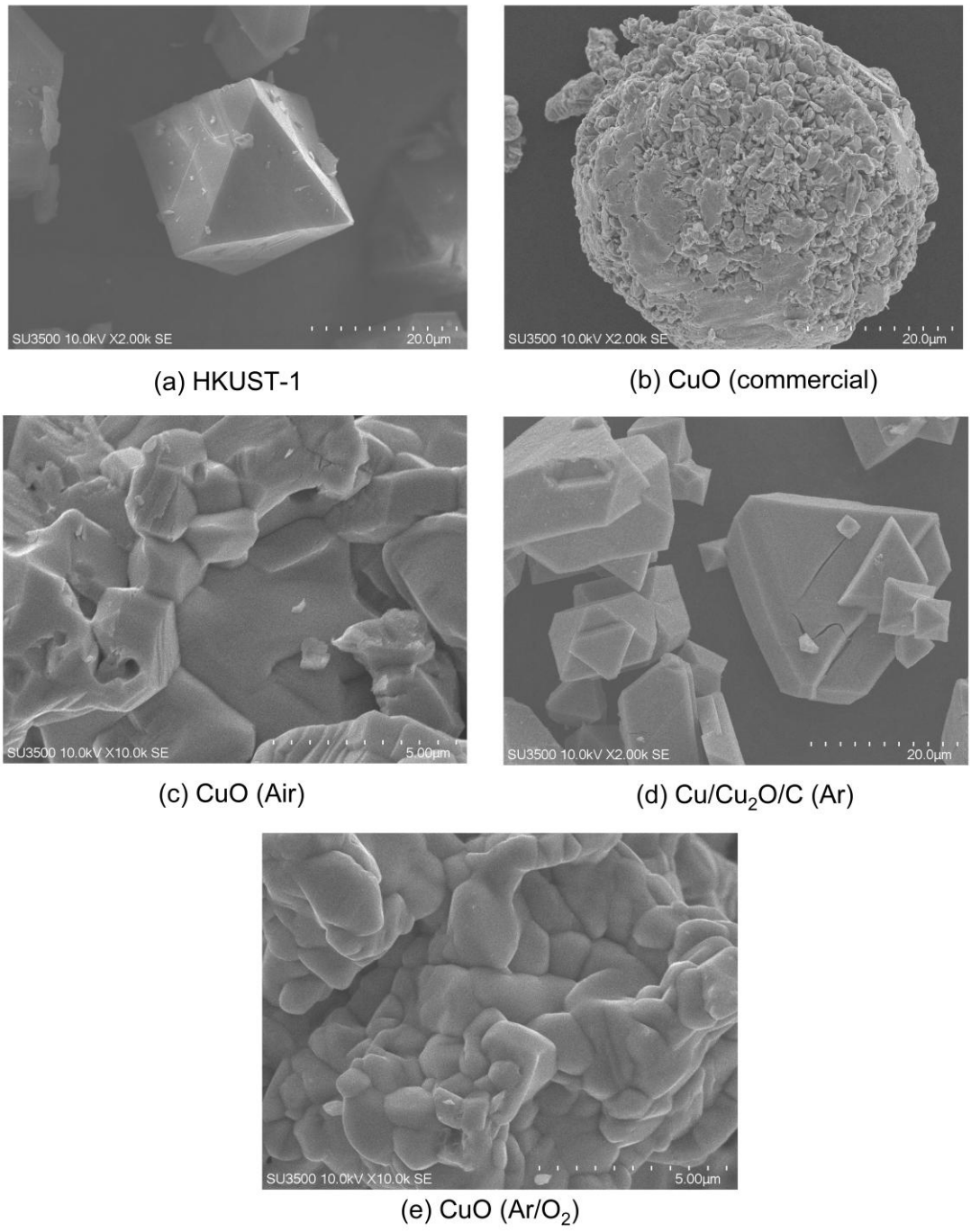

Figure 1. SEM images of the synthesized materials

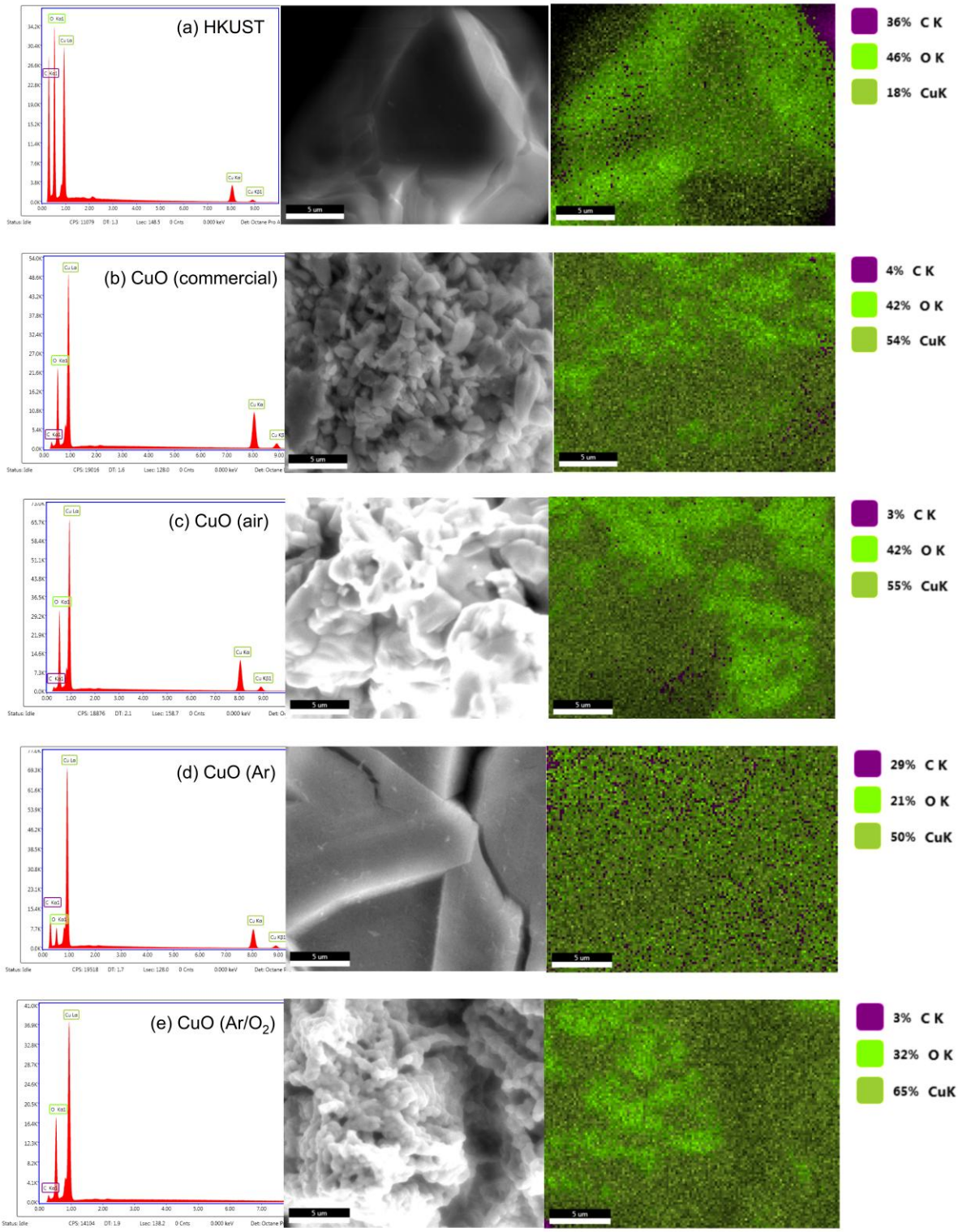

Figure 4. EDX mapping of the synthesized materials.

However These gaseous species diffuse out through the MOF pores, leading to a reduction in the overall carbon content. Concurrently, the remaining Cu^{2+} species react with oxygen to form thermodynamically stable copper oxides at elevated temperatures. As shown in Fig. 4, the carbon content in samples treated under air and Ar/O_2 atmospheres is considerably lower compared to that of the sample treated under pure Ar. Under an inert Ar atmosphere, limited

DOI: https://doi.org/10.25077/jrk.v17i1.822

oxygen availability suppresses complete oxidation, resulting in the retention of residual carbon. Consequently, besides forming Cu/Cu_2O phases, the Ar-treated sample generates a $Cu/Cu_2O/C$ composite due to the presence of unoxidized carbon.

The optical band gap energies of the samples were estimated using the Kubelka-Munk function derived from diffuse reflectance spectra. As summarized in Table 2, the band gap values of CuO (air) and CuO (Ar/O_2) are lower than that of commercial CuO, in agreement with the previous report[26]. The CuO materials derived from HKUST-1 exhibit band gap energies in the range of 1.39–2.04 eV. Notably, the $Cu/Cu_2O/C$ (Ar) sample shows two distinct absorption edges with band gap energies of 2.15 and 2.80 eV, which can be attributed to the coexistence of different phases within the composite.

It can be inferred that interfacial interactions occur between the semiconductor and conductive phases within the composite structure. These interactions modify the electronic structure by introducing intermediate energy states within the band gap, which can influence the recombination dynamics of photogenerated charge carriers. Consequently, electron excitation may proceed via a two-step transition: initially from the valence band (VB) to localized intermediate states, followed by further excitation to the conduction band (CB).

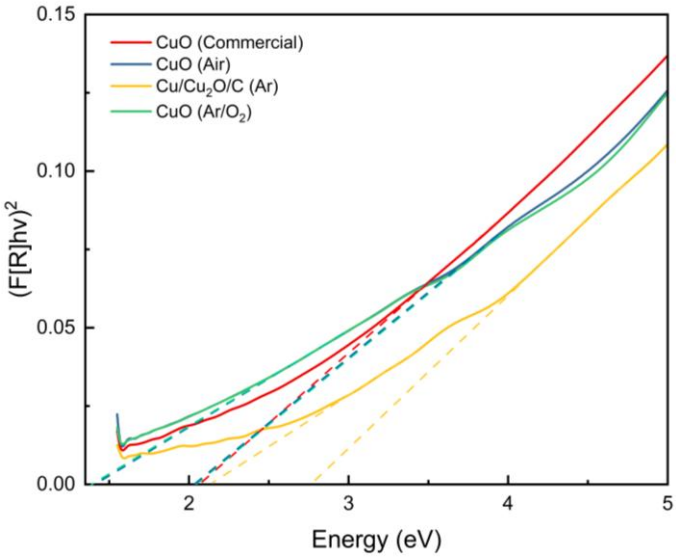

Figure 5. The plot of the Jacobian corrected Kubelka-Munk function for all catalysts.

Table 1. Band gap values of materials

Materials	Band gap (eV)
HKUST-1	2.54
CuO commercial	2.08
CuO (air)	2.03 and 1.41
$Cu/Cu_2O/C$ (Ar)	2.15 and 2.80
CuO (Ar/O_2)	2.04 and 1.39

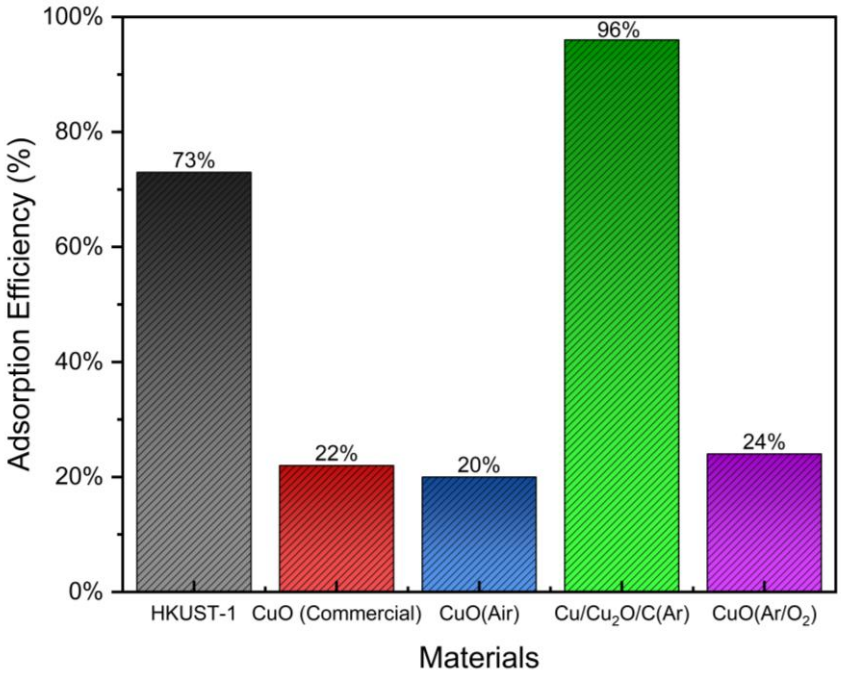

Figure 2. The adsorption efficiency of the material toward CR at the optimum time of 60 minutes.

Table 2. The kinetic adsorption parameters for Congo red removal by each material

Materials	Pseudo-first order model		Pseudo-second order model	
	R^2	Q_{ecal} (mg/g)	R^2	Q_{ecal} (mg/g)
HKUST-1	0.53	43.47	0.97	74.07
CuO commercial	0.71	14.12	0.93	22.37
CuO (air)	0.50	5.08	0.97	17.95
Cu/Cu_2O/C (Ar)	0.54	76.87	0.95	104.16
CuO (Ar/O_2)	0.77	17.96	0.93	26.73

The adsorption performance under dark conditions is presented in Fig. 6. At the optimum contact time of 60 min, the Cu/Cu_2O/C (Ar) sample exhibits the highest adsorption efficiency toward Congo red, reaching 96%, which is significantly higher than that of HKUST-1 (73%). This superior performance can be attributed to the presence of surface crack defects, which increase the accessible surface area, as well as the high carbon content that provides abundant active adsorption sites. These structural and compositional features enhance the interaction between the adsorbent surface and Congo red molecules. In contrast, CuO (air) and CuO (Ar/O_2) show considerably lower adsorption efficiencies of 20% and 24%, respectively, indicating that the absence of residual carbon and the reduced surface defects limit their adsorption capacity.

Contact time is a crucial parameter in evaluating the adsorption kinetics of each material. In this study, the adsorption kinetics of Congo red were analyzed using the pseudo-first-order (Fig. 7a) and pseudo-second-order (Fig. 7b) kinetic models. The corresponding kinetic parameters are summarized in Table 2.

DOI: https://doi.org/10.25077/jrk.v17i1.822

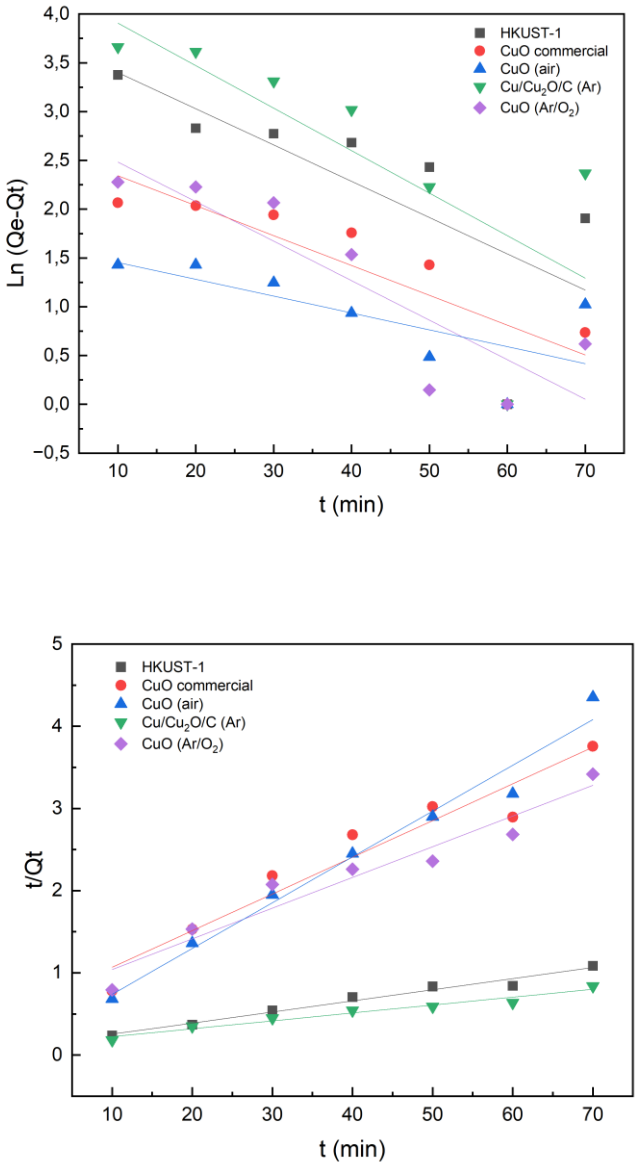

Figure 3. (a) Pseudo-first order adsorption model (b) Pseudo-second order adsorption model.

The pseudo-second-order model provides a better fit to the experimental data than the pseudo-first-order model, as indicated by higher correlation coefficients ($R^2 > 0.93$) for all samples. Additionally, the calculated equilibrium adsorption capacities (Qe cal) from the pseudo-second-order model are in close agreement with the experimental values (Qe exp). These results suggest that the adsorption process is predominantly governed by chemisorption, involving valence forces through electron sharing or exchange between Congo red molecules and the active sites on the adsorbent surface. The adsorption rate is therefore dependent on both the Congo red concentration and the availability of active surface sites. Furthermore, the pseudo-second-order model is widely applied due to its mathematical simplicity and relatively low sensitivity to experimental deviations [27].

The degradation performance, presented in Fig. 8, can be divided into two stages: the dark adsorption stage and the photocatalytic stage under visible-light irradiation.

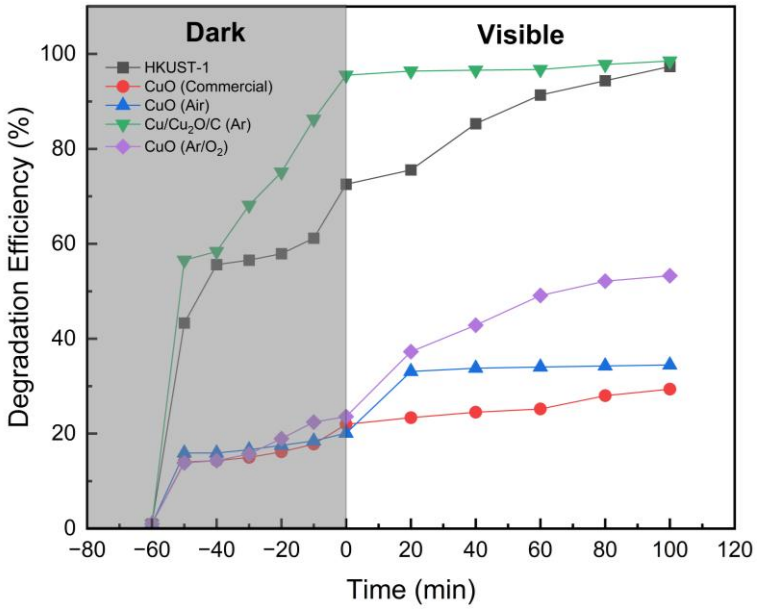

Figure 8. Degradation efficiency of Congo red by various catalysts.

Table 3. Comparison of the present study with other reported photodegradations of CR

Materials	CR (mg/L)	Dosage	UV Source	Adsorption dark condition (%)	Photo-Degradation (%)	Time (min)	Ref.
$CuO/ZnFe_2O_4$	10	75 mg	300 W Xe lamp	28.7	91.1	120	[21]
Cu_2O/Cu_2S-9/1	200	50 mg	Visible light	98.5	99.8	120	[22]
CuO (air)	50	10 mg	Visible light	20	35	100	(This work)
CuO (Ar/O_2)	50	10 mg	Visible light	24	53	100	(This work)
Cu/Cu_2O/C (Ar)	50	10 mg	Visible light	96	99	100	(This work)

During the dark period, the degradation efficiencies vary among the samples due to their different adsorption capacities. Under visible-light irradiation, CuO (air) and CuO (Ar/O_2) exhibit higher degradation efficiencies (35% and 53%, respectively) compared to commercial CuO (29%). The highest overall degradation efficiency (99%) is observed for Cu/Cu_2O/C (Ar). To properly evaluate photocatalytic performance, the enhancement in degradation efficiency from dark to illuminated conditions should be considered. Among the synthesized materials, CuO (Ar/O_2) shows the largest increase, rising from 24% in the dark to 53% under visible light. This improvement can be attributed to its relatively narrow band gap, which facilitates visible-light absorption and enhances charge carrier generation.

Although Cu/Cu_2O/C (Ar) achieves a higher overall degradation efficiency (99%), the increase from dark to light conditions is relatively small (from 96% to 99%), indicating that its performance is predominantly governed by adsorption rather than photocatalysis. Therefore, based on the net photocatalytic contribution, CuO (Ar/O_2) demonstrates superior photocatalytic activity among the synthesized materials.

A comparison of the catalytic performance of the synthesized materials with previously reported catalysts for Congo Red (CR) degradation is summarized in Table 3, demonstrating their superior adsorption and photocatalytic activity under visible-light irradiation.

DOI: https://doi.org/10.25077/jrk.v17i1.822

Table 4. The kinetic adsorption parameters for CR removal by each catalyst

Catalyst	Pseudo-first order model		Pseudo-second order model	
	R^2	Q_{ecal} (mg/g)	R^2	Q_{ecal} (mg/g)
HKUST-1	0.98	52.46	0.99	104.16
CuO commercial	0.90	11.96	0.98	30.48
CuO (air)	0.15	1.07	1.00	33.55
$Cu/Cu_2O/C$ (Ar)	0.67	2.88	0.99	99.00
CuO (Ar/O_2)	0.95	38.95	0.99	59.88

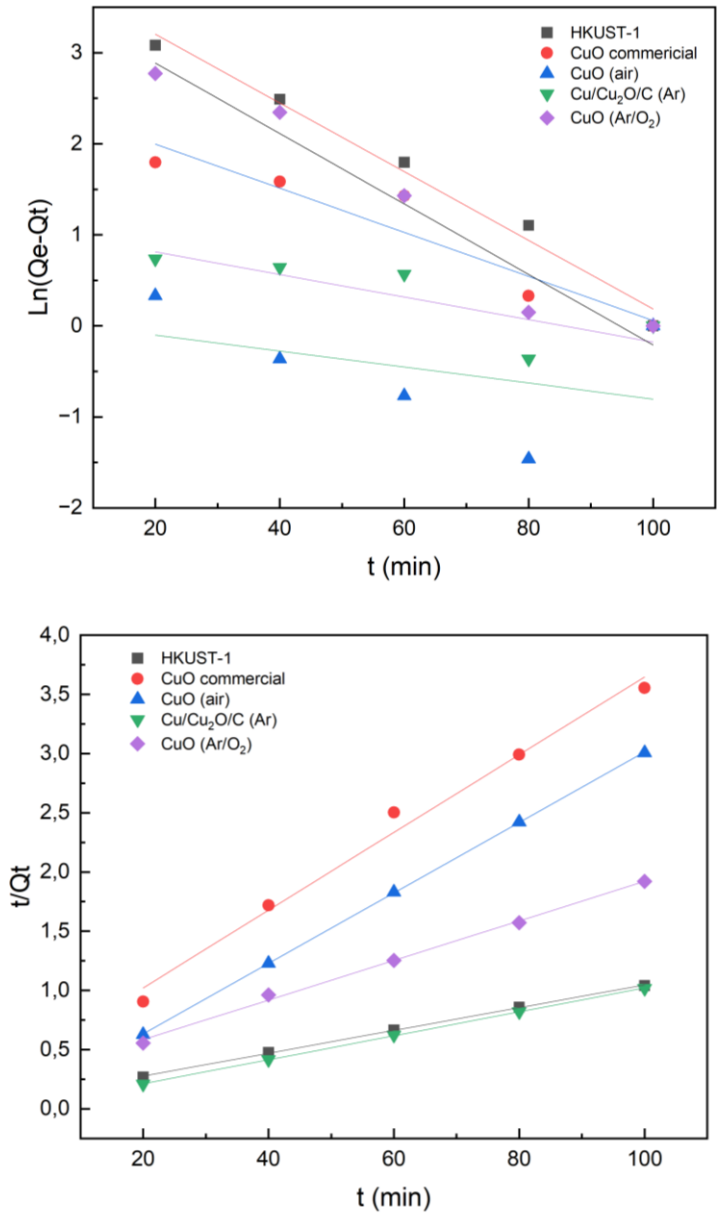

Figure 4. (a) Pseudo-first order photocatalytic model (b) Pseudo-second order photocatalytic model.

The photocatalytic kinetic curve shows that R^2 value of the pseudo-second-order photocatalytic kinetics for all materials is higher than that of the pseudo-first-order kinetics. Therefore, it can be concluded that the photocatalytic degradation of CR by each material follows pseudo-second-order kinetics, as shown in Table 4.

Conclusions

HKUST-1 was successfully synthesized via a solvothermal method at 100 °C for 10 h. Subsequent pyrolysis under different atmospheres led to distinct phase compositions: CuO was obtained under air and Ar/O_2 atmospheres, while treatment under an inert Ar atmosphere produced a $Cu/Cu_2O/C$ composite. The $Cu/Cu_2O/C$ (Ar) sample exhibited the highest adsorption efficiency (96%), demonstrating its excellent performance as an adsorbent compared to the other synthesized materials. In terms of photocatalytic activity, CuO (Ar/O_2) showed the greatest enhancement under visible-light irradiation, with degradation efficiency increasing from 24% (dark condition) to 53% (light condition). These findings indicate that $Cu/Cu_2O/C$ (Ar) is superior for adsorption applications, whereas CuO (Ar/O_2) exhibits the best photocatalytic performance among the synthesized materials.

Acknowledgment

The author extends sincere gratitude to the Ministry of Education, Culture, Research, and Technology of the Republic of Indonesia for its financial support of the 2024 Postgraduate Research (PPS-PTM) under contract number 222/IT1.B07.1/SPP-LPPM/VI/2024, and to SMA BPI 1 Bandung for their valuable collaboration in the practical module testing.

Declaration of Generative AI and AI-Assisted Technologies

The authors declare that no generative AI or AI-assisted technologies were used in the preparation of this manuscript.

Author Contributions

I.M..: Methodology, investigation, data collection, formal analysis, data curation, visualization, writing —original draft preparation, and corresponding author responsibilities. A.P.: Conceptualization, methodology, validation, supervision, and writing —review and editing. Both authors have read and approved the final version of the manuscript.

Funding

This research was funded by Ministry of Education, Culture, Research, and Technology of the Republic of Indonesia, the 2024 Postgraduate Research (PPS-PTM) (contract number 222/IT1.B07.1/SPP-LPPM/VI/2024), and to SMA BPI 1 Bandung.

Declaration of Conflicting Interests

The authors declare no conflict of interest.

References

1. Yoon, Y., Truong, P.L., Lee, D., Ko, & S.H. Metal-Oxide Nanomaterials Synthesis and Applications in Flexible and Wearable Sensors. *ACS Nanosci Au*., 2:64–92 (2022).
2. Khan, S., Noor, T., Iqbal, N., & Yaqoob, L. Photocatalytic Dye Degradation from Textile Wastewater: A Review. *ACS Omega*., 9:21751–21767 (2024).
3. Hua, Z., Pan, Y., & Hong, Q. Adsorption of Congo red dye in water by orange peel biochar modified with CTAB. *RSC Adv*., 13:12502–12508 (2023).
4. Sudirgo, M. M., Surya, R.A., Kristianto, H., *Application of xanthan gum as coagulant-aid for decolorization of synthetic Congo red wastewater*. *Heliyon*., 9:e15011 (2023).
5. Ambigadevi J., Senthil Kumar, P. Enhanced Photocatalytic Removal of Congo Red Dye From Water Environment Using Eggshells Infused With Graphitic Carbon Nitride Composites. *International Journal of Chemical Engineering*., 2025:5541488 (2025).
6. Kim, H, Park, C., Choi, N., & Cho, K. Congo red dye degradation using Fe-containing

 DOI: https://doi.org/10.25077/jrk.v17i1.822

mineral as a reactive material derived from waste foundry dust. *Environ Sci Pollut Res*., 31:28443–28453 (2024).

7. Setyarsih, W., Rohmawati, L., & Ardiansyah, F. F. Photocatalytic Activity of ZnO Nanoparticles from Pineapple Skin for Degradation of Congo Red Dye. *Trends Sci*., 22:9042. (2024).
8. Ljubas, D., Vučemilović, A. & Briševac, D. Optimized Solar-Simulated Photocatalysis of Congo Red Dye Using TiO_2: Toward a Sustainable Water Treatment Approach. *Molecules*, 30:2388 (2025).
9. Panahi Kalamuei M., Motevalli, K., & Aliabadi, M. Rice-like MnO_2 nanoparticles: simple and novel thermal decomposition synthesis, characterization and photocatalytic activity using new precursor. *J Mater Sci: Mater Electron*., 27:4631–4635 (2016).
10. Ishaque, M.Z., Zaman, Y., & Arif, A. Fabrication of ternary metal oxide (ZnO:NiO:CuO) nanocomposite heterojunctions for enhanced photocatalytic and antibacterial applications. *RSC Adv*., 13:30838–30854 (2023).
11. Lim, H., Yusuf, M., & Song, S. Efficient photocatalytic degradation of dyes using photo-deposited Ag nanoparticles on ZnO structures: simple morphological control of ZnO. *RSC Adv* ., 11:8709–8717 (2021)
12. Jalali, N., Rakhsha, A., Nami, M., Photocatalytic activity and pH-induced morphological changes of ZnO/CuO nanocomposites prepared by chemical bath precipitation. *Energy Adv* ., 2:1051–1063 (2023).
13. Shen, K., Chen, X., Chen, J., & Li, Y. Development of MOF-Derived Carbon-Based Nanomaterials for Efficient Catalysis. *ACS Catal*., 6:5887–5903 (2016).
14. Payam, A. F., Khalil, S, Chakrabarti S Synthesis and Characterization of MOF-Derived Structures: Recent Advances and Future Perspectives. Small 20:2310348 (2024).
15. Shahzadi, S., Akhtar, M., Arshad, M., A review on synthesis of MOF-derived carbon composites: innovations in electrochemical, environmental and electrocatalytic technologies. *RSC Adv*., 14:27575–27607 (2024).
16. Łuczak, J., Kroczewska, M., Baluk, M. Morphology control through the synthesis of metal-organic frameworks. *Advances in Colloid and Interface Science*., 314:102864 (2023).
17. Sáenz García, D. R., Turnes Palomino, G., Leal, L.O., Palomino Cabello, C. Tailoring ZIF-8-derived carbons through surface modifications for enhanced pharmaceutical removal. *Microporous and Mesoporous Materials*., 404:114043 (2026).
18. Li, J. Huang R, Chen L, et alMixed valence copper oxide composites derived from metal–organic frameworks for efficient visible light fuel denitrification. RSC Adv 13:36477–36483 (2023).
19. Hendri, Y.N., Rati, Y., Auni, A. K. E. Controlled pyrolysis of Zn-based metal organic framework-derived ZnO/C for Rhodamine-B degradation. *Materials Today Communications*., 37:107011 (2023).
20. Abuzeid, H. M., Youssef, A. M., & Yakout, S. M. Green Synthesized α-MnO_2 As a Photocatalytic Reagent for Methylene Blue and Congo Red Degradation. *Journal of Elec Materi*., 50:2171–2181 (2021).
21. Yang, A., Li, P., & Zhong, J. Facile preparation of low-cost HKUST-1 with lattice vacancies and high-efficiency adsorption for uranium. *RSC Adv*., 9:10320–10325 (2019).
22. Yan, J., Wang, H., & Jin, B. Cu-MOF derived $Cu/Cu_2O/C$ nanocomposites for the efficient thermal decomposition of ammonium perchlorate. *Journal of Solid State Chemistry*., 297:122060 (2021).
23. Balık, M., Bulut, V., Erdogan, I.Y. Optical, structural and phase transition properties of Cu_2O, CuO and Cu_2O/CuO: Their photoelectrochemical sensor applications. *International Journal of Hydrogen Energy*., 44:18744–18755 (2019).

24. Yang, Y., Dong, H., Wang, Y. A facile synthesis for porous CuO/Cu_2O composites derived from MOFs and their superior catalytic performance for CO oxidation. *Inorganic Chemistry Communications.,* 86:74–77 (2017).

25. Karimzadeh, M., Niknam, K., Manouchehri, N., & Tarokh D. A green route for the cross-coupling of azide anions with aryl halides under both base and ligand-free conditions: exceptional performance of a Cu_2 O–CuO–Cu–C nanocomposite. *RSC Adv.,* 8:25785–25793 (2018).

26. Sagadevan, S., Pal, K., & Chowdhury, Z. Z. Fabrication of CuO nanoparticles for structural, optical and dielectric analysis using chemical precipitation method. *J Mater Sci: Mater Electron.,* 28:12591–12597 (2017).

27. Ambigadevi, J., & Senthil Kumar, P. Enhanced Photocatalytic Removal of Congo Red Dye From Water Environment Using Eggshells Infused With Graphitic Carbon Nitride Composites. *International Journal of Chemical Engineering.,* 2025:5541488. (2025).

 DOI: https://doi.org/10.25077/jrk.v17i1.822